

Cortical functional hyperconnectivity in a mouse model of depression and selective network effects of ketamine

Alexander McGirr,^{1,2} Jeffrey LeDue,^{1,2} Allen W. Chan,^{1,2} Yicheng Xie^{1,2} and Timothy H. Murphy^{1,2}

See Huang and Liston (doi:10.1093/awx166) for a scientific commentary on this article.

Human depression is associated with glutamatergic dysfunction and alterations in resting state network activity. However, the indirect nature of human *in vivo* glutamate and activity assessments obscures mechanistic details. Using the chronic social defeat mouse model of depression, we determine how mesoscale glutamatergic networks are altered after chronic stress, and in response to the rapid acting antidepressant, ketamine. Transgenic mice (Ai85) expressing iGluSnFR (a recombinant protein sensor) permitted real-time *in vivo* selective characterization of extracellular glutamate and longitudinal imaging of mesoscale cortical glutamatergic functional circuits. Mice underwent chronic social defeat or a control condition, while spontaneous cortical activity was longitudinally sampled. After chronic social defeat, we observed network-wide glutamate functional hyperconnectivity in defeated animals, which was confirmed with voltage sensitive dye imaging in an independent cohort. Subanaesthetic ketamine has unique effects in defeated animals. Acutely, subanaesthetic ketamine induces large global cortical glutamate transients in defeated animals, and an elevated subanaesthetic dose resulted in sustained global increase in cortical glutamate. Local cortical inhibition of glutamate transporters in naïve mice given ketamine produced a similar extracellular glutamate phenotype, with both glutamate transients and a dose-dependent accumulation of glutamate. Twenty-four hours after ketamine, normalization of depressive-like behaviour in defeated animals was accompanied by reduced glutamate functional connectivity strength. Altered glutamate functional connectivity in this animal model confirms the central role of glutamate dynamics as well as network-wide changes after chronic stress and in response to ketamine.

1 Department of Psychiatry, University of British Columbia, Vancouver, BC, Canada

2 Djavad Mowafaghan Centre for Brain Health, University of British Columbia, Vancouver, BC, Canada

Correspondence to: Alexander McGirr
2255 Wesbrook Mall, Vancouver, BC, V6T 1Z3, Canada
E-mail: alexander.mcgirr@alumni.ubc.ca

Correspondence may also be addressed to: Timothy Murphy
E-mail: thmurphy@mail.ubc.ca

Keywords: associational areas; affective disorders; drug treatment; imaging

Abbreviations: CSD = chronic social defeat; TST = Tail Suspension Test; VSD = voltage sensitive dye

Introduction

Major depressive disorder is a common illness (WHO, 2008), affecting 5–15% of the population across the lifespan. Moreover, its relapsing remitting course defines 20–30% of affected individuals and, among patients who are treated for the first time with effective treatments, only 50% will exhibit a significant reduction in symptoms (Rush *et al.*, 2006). Accordingly, a major and evolving research focus with the goal of guiding and refining treatment is the identification of the biological substrate of depression and mechanisms of antidepressant response through neuroimaging. Increasingly, our understanding of human major depressive disorder suggests a distributed network disturbance (Gong and He, 2015; Smart *et al.*, 2015) and glutamatergic dysfunction (Yuksel and Ongur, 2010; Luykx *et al.*, 2012); however, these remain independent observations.

Utilizing *in vivo* mesoscale imaging to probe extracellular glutamate functional connectivity, we characterize network alterations in a mouse model of depression, the acute effects of subanaesthetic ketamine, and the longitudinal course of the accompanying network changes. To achieve this, we used *in vivo* millisecond-timescale widefield imaging of spontaneous cortical activity using an extracellular glutamate sensor (iGluSnFR) (Marvin *et al.*, 2013) in the transgenic Ai85 mouse (Madisen *et al.*, 2015) permitting longitudinal imaging through an intact skull (Silasi *et al.*, 2016; Xie *et al.*, 2016). This approach provides incisive characterization of mesoscale functional extracellular glutamate circuits (Xie *et al.*, 2016) through *in vivo*, real time, *in situ* extracellular glutamate imaging with high spatial and temporal resolution in the cortex (Marvin *et al.*, 2013; Xie *et al.*, 2016).

One of the most common methods of studying large-scale functional networks involves capitalizing on spontaneous neuronal activity, a ubiquitous phenomenon that reveals intricate topographical organization (Bullmore and Sporns, 2012). In humans, resting state analyses through functional MRI have demonstrated slow (<0.1 Hz) regional blood oxygen level fluctuations supporting large-scale resting state networks (Fox and Raichle, 2007). In animal models, as in humans, studying spontaneous cortical activity in the absence of motor planning and sensory experience provides a powerful method for characterizing functional connectivity and network alterations (Mohajerani *et al.*, 2013; Lim *et al.*, 2015). Reproducing a depression-like phenotype in a tractable animal model enables the identification and manipulation of large-scale circuit interactions to establish a common mechanism with significantly refined spatial and temporal resolution. The default mode network, in particular, appears to be intimately related to psychiatric illnesses (Menon, 2011). Most consistent within the human resting state major depressive disorder imaging literature is hyperconnectivity within the default mode network (Kaiser *et al.*, 2015),

hypothesized to reflect a ruminative egocentric state (Buckner *et al.*, 2008; Hamilton *et al.*, 2015).

Among the antidepressant manipulations with the ability to inform large-scale glutamatergic network interactions in depression, the rapid acting antidepressant properties of subanaesthetic ketamine hold significant promise. Unlike conventional treatments, this agent with both NMDA receptor and non-NMDA receptor actions (Zanos *et al.*, 2016) results in robust antidepressant effects within minutes to hours in humans (McGirr *et al.*, 2015; Xu *et al.*, 2016), providing a unique window for capturing functional network changes and improving mechanistic understanding. Moreover, though there have been several high quality characterizations of key nodes and circuits (Li *et al.*, 2010; Autry *et al.*, 2011; Fuchikami *et al.*, 2015; Carreno *et al.*, 2016; Chowdhury *et al.*, 2017), subanaesthetic ketamine produces global cortical increases in brain-derived neurotrophic factor (BDNF) (Autry *et al.*, 2011), highlighting that a distributed network undergoes rapid change.

Here, we longitudinally characterize inter-regional correlations of extracellular glutamate to reflect functional connectivity in an animal model of depression, and the unique extracellular glutamate effects of subanaesthetic ketamine after chronic social defeat (CSD).

Materials and methods

Animals

We studied transgenic mice developed by the Allen Institute for Brain Science using an intersectional genetic strategy to achieve cell-type specific expression of neural sensors in the Ai85 and Ai94 lines (Madisen *et al.*, 2015). EMX-CaMKII-iGluSnFR transgenic mice (Fig. 1A) expressing iGluSnFR in excitatory cortical neurons were generated by crossing homozygous B6.129S2-Emx1^{tm1^(cre)Krj}/J strain (Jax #005628) and B6.Cg-Tg(CamK2a-tTA)1Mmay/DboJ strain (Jax #007004) with hemizygous B6; 129S-Igs7^{tm85^(tetO-iGluSnFR)Hze}/J strain (Jax #026260) (Madisen *et al.*, 2015; Xie *et al.*, 2016). A subset of transgenic EMX-CaMKII-GCaMP6s mice was used in conjunction with optical mapping. These mice were generated by crossing homozygous B6.129S2-Emx1^{tm1^(cre)Krj}/J (Jax #005628) and B6.Cg-Tg(Camk2a-tTA)1Mmay/DboJ (Jax #007004) with hemizygous B6.Cg-Igs7^{tm94.1^(tetO-GCaMP6s)Hze}/J (Jax #024104) (Madisen *et al.*, 2015).

To validate iGluSnFR findings, we also characterized an independent cohort of adult male (8 weeks old) C57BL/6J mice (Charles River) with voltage sensitive dye (VSD) experiments. Male Thy1-GFP mice (8–12 weeks old) were studied as activity-independent fluorescence controls.

The housing facility had a 12:12 light cycle and experiments were performed during the latter part of the light cycle. Prior to CSD, mice were housed in groups of two to five. All mice had *ad libitum* access to water and standard laboratory mouse diet. The animal protocols were approved by the University of British Columbia Animal Care Committee and were in accordance with guidelines set forth by the Canadian Council for Animal Care.

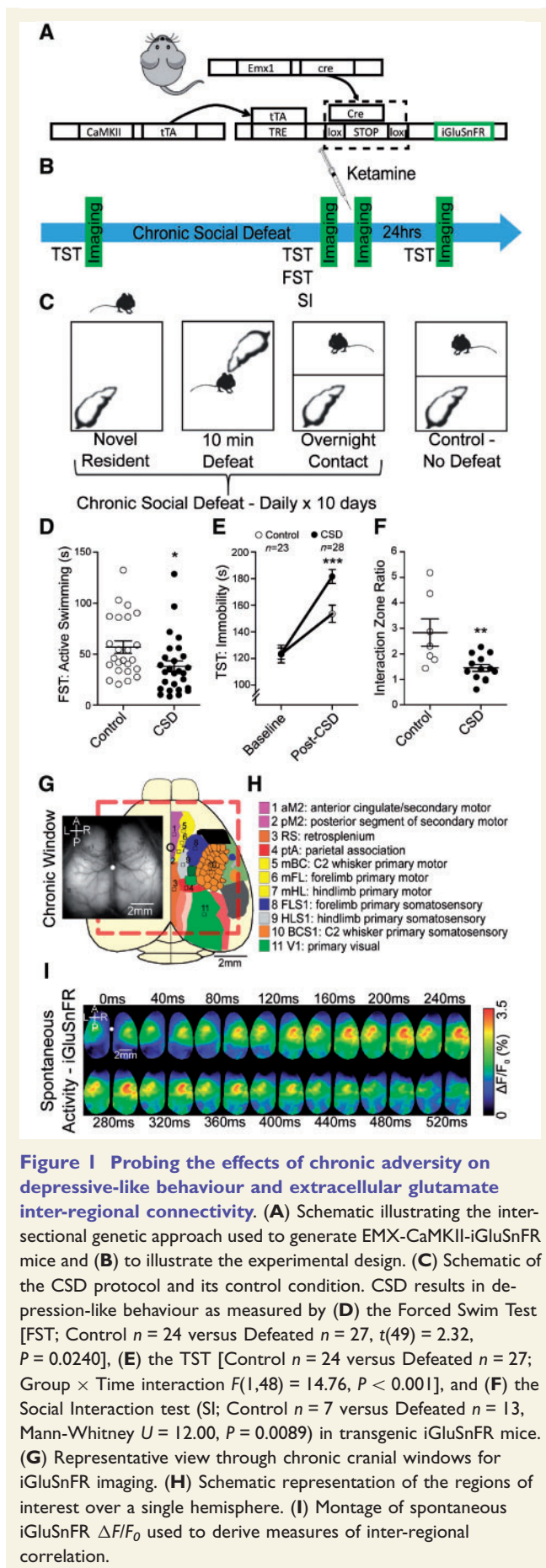


Figure 1 Probing the effects of chronic adversity on depressive-like behaviour and extracellular glutamate inter-regional connectivity. **(A)** Schematic illustrating the inter-sectional genetic approach used to generate EMX-CaMKII-iGluSnFR mice and **(B)** to illustrate the experimental design. **(C)** Schematic of the CSD protocol and its control condition. CSD results in depression-like behaviour as measured by **(D)** the Forced Swim Test [FST; Control $n = 24$ versus Defeated $n = 27$, $t(49) = 2.32$, $P = 0.0240$], **(E)** the TST [Control $n = 24$ versus Defeated $n = 27$; Group \times Time interaction $F(1,48) = 14.76$, $P < 0.001$], and **(F)** the Social Interaction test (SI; Control $n = 7$ versus Defeated $n = 13$, Mann-Whitney $U = 12.00$, $P = 0.0089$) in transgenic iGluSnFR mice. **(G)** Representative view through chronic cranial windows for iGluSnFR imaging. **(H)** Schematic representation of the regions of interest over a single hemisphere. **(I)** Montage of spontaneous iGluSnFR $\Delta F/F_0$ used to derive measures of inter-regional correlation.

Chronic social defeat

We performed CSD as described by Golden *et al.* (2011). Four-month-old male CD1 mice (Charles River) served as resident mice. Eight-week-old male mice (Ai85-iGluSnFR, Ai94-GcaMP6s, and C57BL/6J strains) were introduced into the resident CD1's cage, where they experienced physical defeat for 10 min prior to being separated by a perforated Plexiglas® divider and maintained in sensory contact overnight. Every day for 10 days, mice were transferred to a different cage to experience physical defeat by a new resident mouse, and similarly maintained in sensory contact overnight. Control mice were maintained separated by a divider and rotated daily without experiencing physical defeat. Following the CSD and control protocols, animals were single housed for the remainder of the protocol. Behavioural tests were performed every other day.

Forced swim test

Mice were placed into a transparent glass beaker (25 cm height, 18 cm diameter), containing water at 24–25°C. For 5 min, the mice remained in the water while an observer coded their active swimming and floating (including efforts to maintain position) (Porsolt *et al.*, 1977). The water was changed between animals. Only the last 4 min of the experiment are reported.

Tail suspension test

Mice were suspended by the tail, which was affixed to a 6 cm ledge at 50 cm elevation using adhesive tape placed at 2 cm from the tip of the tail. During the 5-min trial, an observer coded their behaviour and quantified the time spent immobile (Steru *et al.*, 1985). Immobility is reported for the entire duration of the trial.

Sucrose preference test

Mice were single-housed without prior food or water deprivation. They were habituated to the presence of two bottles for 24 h, which were replaced with fresh bottles containing water and a 1% sucrose solution for 16 h. The bottles were pseudorandomly ordered. At the conclusion of the testing period, the bottles were weighed, and the sucrose preference was calculated as a ratio of the sucrose solution to water consumed. As we were unable to demonstrate a sucrose preference in Ai85 control mice, data are only presented for C57BL/6J mice.

Social interaction test

This test was carried out as described by Golden *et al.* (2011). We custom 3D printed a white plastic enclosure (6-cm width, 8-cm depth, 15-cm height) constituted of honeycomb openings (1.5 cm), which was placed in the centre of the far wall of a 42 cm \times 42 cm arena. Under infrared illumination, we filmed two 150 s epochs in which the enclosure was either empty ('no target') or contained a novel CD1 mouse ('target') using the Raspberry Pi single board computer and its Picam module. The test mouse was first introduced to the arena for the no target trial, and then the target trial. Using custom written

MATLAB (Mathworks, Natick, MA) software, we defined the interaction zone as an 8 cm area surrounding the outer limit of the enclosure, and the social interaction ratio defined as the ratio of the time spent in the interaction zone for the ‘target’ and ‘no target’ trials.

Drugs

Subanaesthetic doses (10 mg/kg or 50 mg/kg, 200 μ l volume, intraperitoneal) and, for a subset, anaesthetic doses (100 mg/kg, 200 μ l volume, intraperitoneal), of racemic ketamine hydrochloride (Bioniche) were administered in saline dilution. The short acting benzodiazepine, midazolam (2 mg/kg, 200 μ l volume, intraperitoneal; Sandoz), was similarly administered to a subset of animals. The competitive non-transportable blocker of excitatory amino acid transporters, DL-theo- β -benzyloxy-spartic acid (DL-TBOA, Tocris Bioscience) was kept at -20°C in dimethyl sulphoxide (DMSO) stock solution and diluted in HEPES-buffered saline (500 μM , final DMSO concentration 0.5%) before incubating over the cortex for 30 min prior to experiments.

Chronic window surgery

Chronic window surgeries were performed in 7-week-old mice as described by Silasi *et al.* (2016). After exposing the skull by removing a skin flap from 3 mm anterior to bregma to posterior end of skull and down lateral to eye level, a metal screw was attached to the skull prior to embedding it in transparent dental cement (C&B-Metabond, Parkell). The space between a flat 9×9 mm glass coverslip (tapered by 2 mm anteriorly) and the skull is filled with the transparent dental cement. The window extends to the attachment of the temporalis muscle, therefore maximizing the visualized cortex while minimizing functional impairment relating to the window. Mice were allowed to recover for 7 days prior to any interventions or imaging.

Image acquisition

Animals were imaged under 1.0% isoflurane (1.5% for Ai94 mice) with body temperature maintained at 37°C , and a subset of animals were imaged during quiet wakefulness. For iGluSnFR and VSD data collection, 12-bit images were captured with 6.67-ms (150 Hz) temporal resolution with a charge-coupled device (CCD) camera (1M60 Pantera, Dalsa) and an EPIX E4DB frame grabber with XCAP 3.1 imaging software (EPIX, Inc). For GCAMP6s experiments, temporal resolution was 10 Hz. The focus was 800 μm below the surface to reduce signal distortion due to large cortical blood vessels. Images were taken through a microscope composed of front-to-front video lenses (8.6×8.6 mm field of view, 67 μm per pixel). Quantification of image stability using slice alignment (Tseng *et al.*, 2012) confirmed minimal head motion during our anaesthetized recordings ($n = 5$, 67 $\mu\text{m}/\text{pixel}$; x -axis 0.021 ± 0.019 pixels, range: 0.0018–0.031 pixels; y -axis 0.061 ± 0.019 , range: 0.051–0.080 pixels).

Spontaneous cortical activity

For each recording, spontaneous brain activity was captured with 6.67 ms (150 Hz) temporal resolution for a total of 50 000 frames. Excitation illumination was initiated 5 s prior

to all acquisitions for visual habituation. We imaged with 20 ms (50 Hz) temporal resolution during the 5 min preceding and 15 min following the injection of ketamine (with a brief interruption for the injection itself), before once again imaging with 6.67 ms temporal resolution for inter-regional correlation analyses.

iGluSnFR imaging and processing

For iGluSnFR excitation, we used LED illumination (Luxeon, 470 nm) and a 467–499 nm excitation filter. iGluSnFR fluorescence emission was filtered using a 510–550 nm bandpass filter (Chroma). iGluSnFR signals were expressed as $\Delta F/F_0$, a percentage change relative to the mean $[(F - F_0)/F_0 \times 100\%]$, where F represents the fluorescence signal at any given time and F_0 represents the average of fluorescence over all frames] using MATLAB.

Because of the optical properties of haemoglobin in the blue-green part of the spectrum (Ma *et al.*, 2016), care must be taken to avoid contamination of the iGluSnFR signal with blood volume or other (such as heartbeat-related) haemodynamic effects. While global signal regression can address some of these issues, we chose to avoid its use because of the controversial possibility of anti-correlated networks associated with this method (Fox *et al.*, 2009) and, more importantly, the inability to reliably compare recordings from the same animal across time. Instead we temporally filtered the signal at 0.3–3 Hz. This filter is sufficient to produce recordings that lack the haemodynamic confounds blue-green reporters such as iGluSnFR are prone to; however, a small number of recordings were excluded from analyses when this bandpass proved qualitatively insufficient. One defeated animal was excluded from all regional correlation analyses as complete matrices could not be generated due to obstruction.

Voltage sensitive dye surgery

To validate iGluSnFR findings, we performed *in vivo* VSD imaging using an acute surgical preparation (Mohajerani *et al.*, 2010, 2011, 2013; Lim *et al.*, 2014; Chan *et al.*, 2015). At 10 weeks of age, mice underwent a craniotomy under isoflurane (1.0–1.5%) with buprenorphine (0.05 mg/kg intraperitoneally). Body temperature was maintained at 37°C using a heating pad with a feedback thermistor. The skull was exposed and fastened to a steel plate. We performed a large 7×8 mm craniotomy (bregma 2.5 to -4.5 mm, lateral 0–4 mm) overlying both cortical hemispheres, and removed the underlying dura. We used RH-1692 dye (Optical Imaging), which was dissolved in HEPES-buffered saline solution (1 mg/ml). RH-1692 was incubated over the cortex for 60–90 min to allow staining of all neocortical layers. Unbound RH-1692 was washed prior to covering the surface of the brain with 1.5% agarose made in HEPES-buffered saline and a glass coverslip.

Voltage sensitive dye imaging and processing

For VSD excitation, we used a red LED (Luxeon, 627 nm) and 630 ± 15 nm filters. VSD fluorescence was filtered using a

673–703 nm bandpass optical filter (Semrock). To reduce regional bias in VSD signal caused by uneven dye loading or brain curvature, all VSD responses were expressed as a percentage change ($\Delta F/F_0 \times 100\%$) using MATLAB. VSD fluorescence was temporally filtered in MATLAB using a zero-phase lag Chebyshev bandpass filter (zero-phase filter) at 0.3–3 Hz.

Viral injection and expression confirmation

Viral delivery of the red shifted opsin, ChrimsonR (Klapoetke *et al.*, 2014) (AAV9.Syn.ChrimsonR-tdTomato.WPRE.bGH, Penn Vector Core), involved syringe infusion pump injection (UMC4; World Precision Instruments). Mice were injected with 1 μ l to a depth of \sim 350 μ m and speed of 1 nl/s. Four-week-old mice were injected for sufficient ostial recovery and chronic window implantation at 7 weeks of age, with CSD at 8 weeks. Under 1.5% isoflurane, injections were performed at three sites: (i) motor cortex (1 mm anterior and 2 mm lateral to bregma); (ii) somatosensory cortex (1.5 mm posterior and 2.5 mm lateral to bregma); and (iii) visual cortex (3.5 mm posterior and 2 mm lateral to bregma).

At the conclusion of mapping experiments, animals were transcardially perfused with 4% paraformaldehyde (Sigma-Aldrich). The fluorophores were imaged using standard Carl Zeiss AG filter sets (38 HE, 489038-9901-000; and 43 HE, 489043-9901-000).

Sensory evoked mapping

At the post-CSD/control time point, after acquiring spontaneous brain activity, we presented 10 sensory stimuli (to forelimb, hindlimb, whisker, and a visual flash) for cortical mapping and region of interest identification. Limb stimulation involved thin acupuncture needles (0.14 mm) inserted subcutaneously and 1 mA, 1 ms electrical stimulation. For whisker stimulation, we used a piezoelectric bending actuator attached to the C2 whisker. Visual stimulation used a 535 nm LED pulse of light directed towards the animal's eye. Responses to sensory stimuli were calculated as the normalized difference to the average of five stimulus-free trials ($\% \Delta F/F_0$) in MATLAB (MathWorks).

Sensory mapping in Ai94 mice was performed using a piezoelectric bending actuator for limb and whisker stimulation with 100 ms 50 Hz trains. We presented 20 sensory stimuli and the responses were calculated as the normalized difference to the average of 10 stimulus-free trials interleaved with stimulus trials.

Optical mapping

We performed optical mapping using the red-shifted opsin ChrimsonR (Klapoetke *et al.*, 2014) in Ai85 and Ai94 mice at two time points: (i) pre-; and (ii) post-CSD/control. We used a diode pumped solid state laser delivering a 589 nm 200 μ m diameter laser beam (CNI, Optoelectronics). We averaged responses from 20 trials to each region of interest using a 5 ms 12.5 mW pulse for Ai85 mice and a 200 ms 50 Hz train of 1 ms 12.5 mW pulses for Ai94 mice. We first acquired sensory responses from which parietal temporal association and retrosplenial cortex were identified using stereotactic coordinates

(Allen Institute for Brain Science). Responses to stimulation were calculated as the normalized difference to the average of 10 stimulus-free trials ($\% \Delta F/F_0$) in MATLAB (MathWorks). Custom-written MATLAB scripts (Lim *et al.*, 2014) were used to analyse and quantify the peak amplitude in the 200 ms following stimulation for the Ai85 line and 1.5 s for the Ai94 line.

Theo- β -benzyloxyspartic acid imaging

Female Ai85 mice (8–12 weeks) were anaesthetized, received analgesia, and their skull was fastened to a steel plate. A barrier composed of dental cement (1 mm width \times 2.5 mm elevation) was erected along the sagittal suture. Two 2 mm craniotomies were performed over both the left and right sensorimotor cortices. These 'wells' were filled with HEPES-buffered saline. To ensure accurate solution concentration, the 'well' was thrice replaced with 500 μ M DL-TBOA solution (0.5% DMSO), and the contralateral 'well' was thrice replaced with 0.5% DMSO HEPES-buffered saline. After 30 min of incubation, ketamine (10 mg/kg or 50 mg/kg, intraperitoneal) was administered and imaging acquired with 20 ms (50 Hz) temporal resolution for the 5 min preceding and 15 min following the injection, before imaging with 6.67 ms temporal resolution.

Network analysis

Matrices (22 \times 22) were created based on zero-lag correlation of spontaneous iGluSnFR or VSD $\Delta F/F_0$ activity from 22 regions of interest (11 \times 5 pixel regions of interest per hemisphere). Region of interest coordinates were derived from sensory evoked responses and stereotactic coordinates in relation to these (Allen Institute for Brain Science). These regions of interest are graphically represented in Fig. 1G. We characterized the following regions of interest: aM2 = secondary motor/anterior cingulate, pM2 = posterior secondary motor, RS = retrosplenium, ptA = parietal association area, mBC = barrel motor, mFL = forelimb motor, mHL = hindlimb motor, FLS1 = forelimb sensory, HLS1 = hindlimb sensory, BCS1 = barrel sensory, and V1 = primary visual cortex.

Self-correlation among regions of interest was omitted as were symmetrical correlations obtained across the diagonal (upper triangle of correlation values in correlation matrices). We used modified custom written MATLAB scripts (Lim *et al.*, 2015) (http://www.neuroscience.ubc.ca/faculty/murphy_software.html) as well as the Bioinformatics and Brain Connectivity Toolbox (Rubinov and Sporns, 2010) to create a network diagram based on the differences in conditions. Node size is proportional to the strength of the connections per node and edge thickness between nodes is proportional to the weight of the connections between nodes. For the purposes of visualization, we only display relative values exceeding a prespecified threshold in the main figures. Full matrices are available in the Supplementary material.

Network validation

We sought to validate iGluSnFR networks using k-means clustering (eight clusters) in anaesthetized and awake animals. We characterized the stability of correlation estimates in awake recordings by habituating 8-week-old mice to head fixation

over 3 days before acquiring spontaneous cortical activity on two sequential days. Node correlations were calculated as above, and change between imaging sessions was determined for each mouse.

Seed-pixel correlation maps

Zero-lag cross-correlation coefficient r -values between the temporal profiles of a single selected pixel (derived from maximal responses to sensory evoked stimuli or stereotaxic coordinates) and the entire imaging field were calculated. For presented maps, spatial smoothing (Gaussian blur, $\sigma = 134 \mu\text{m}$) was applied.

Time course analysis

The iGluSnFR signal observed in response to acute ketamine consists of slowly rising fluorescence intensity and fluorescence transients. We therefore used two strategies to examine these changes: (i) a MATLAB implementation of a smoothing function (5000 time points at 50 Hz) for averaged time course of iGluSnFR fluorescence; and (ii) a MATLAB implementation of a rolling ball filter in the time domain to decompose the signal into the slowly rising fluorescence intensity, and the fluorescence transients. To accomplish decomposition of the signal we set the rolling ball radius to 20 s (1000 time points at 50 Hz or 3000 time points at 150 Hz), effectively low passing the slowly rising fluorescence into one signal and, by subtraction from the original, high passing the transients into a second signal. Thus, the original time courses can be easily recovered by the addition of the high and low pass components from the rolling ball filter. Analyses of transients focused on the high pass component, and defined according to a threshold set at 3 standard deviations (SD) above the defeated animals' normalized fluorescence level, which effectively minimized the number of 'transients' meeting threshold in the baseline condition.

Statistics

Cross-sectional analysis used Student's t -test or ANOVA for normally distributed data or Mann-Whitney test for non-normally distributed data. Paired samples (DL-TBOA, midazolam and deep anaesthesia experiments) used paired t -tests. Behaviour with multiple time points was analysed with two-group repeated measures ANOVA. The cumulative distribution functions of correlation parameters derived from matrices were generated for qualitative examination for baseline to post-CSD/control, and with vehicle-treated groups thereafter. We used general linear mixed-effects models (GLMEM) predicting correlation values with a fixed effect for group or time point, respectively, including random effects for inter-regional correlations. Significance was set at $\alpha \leq 0.05$. We further used bootstrapping (resampling with replacement, 1000 samples) to determine 95% confidence intervals (CI) of condition mean differences.

Results

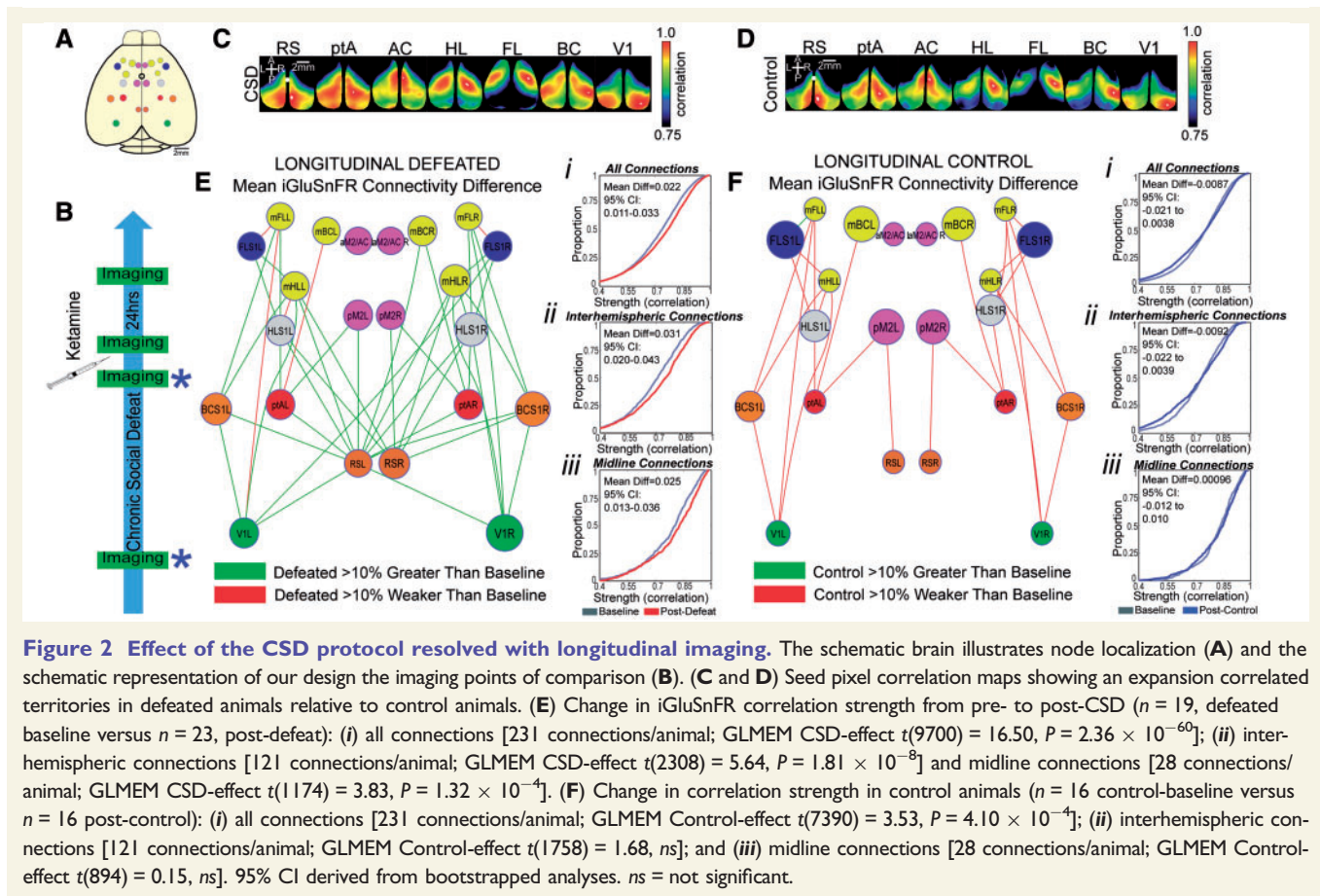
Our methodological design is illustrated in Fig. 1B. The CSD model of depression (Fig. 1C) resulted in depressive-

like behaviour as measured by the Forced Swim Test (Fig. 1D), Tail Suspension Test (TST) (Fig. 1E) and Social Interaction Test (Fig. 1F). For parsimony, we hereafter refer to animals having undergone the CSD protocol as 'defeated'.

We used *in vivo* millisecond-timescale wide-field imaging approaches to capture task-independent spontaneous cortical activity with chronic imaging of extracellular glutamate sensor through an intact skull (iGluSnFR; representative transcranial chronic window Fig. 1G). With continuous high speed sampling ($67 \mu\text{m}/\text{pixel}$, 150 Hz) over a wide expanse of cortex, we defined 22 regions of interest (5×5 pixels; 11/hemisphere; Fig. 1H) and measure functional connectivity strength using zero-lag correlation of region of interest time courses (Lim *et al.*, 2015). The spatial and temporal resolution of the associated $\Delta F/F_0$ signal used to quantify region of interest functional correlation is illustrated in montages (Fig. 1I) and sample videos (Supplementary Videos 1 and 2). We focused on assessment of spontaneous activity to better align our results with human resting state findings, and though our experiments were performed under anaesthesia, these networks are persistent across states devoid of motor or sensory activity, such as anaesthesia, natural sleep and quiet wakefulness (Vincent *et al.*, 2007; Horowitz *et al.*, 2008). Indeed, spontaneous iGluSnFR activity revealed topographical organization in both the awake and anaesthetized state (Supplementary Fig. 1A and B) consistent with the rodent default mode network identified with functional MRI (Lu *et al.*, 2012). Moreover, the region of interest connection strengths identified through zero-lag correlation over imaging sessions in the awake state, without the repeated stress of induction and anaesthesia, were stable (Supplementary Fig. 1C).

Increased regional iGluSnFR functional correlation after chronic social defeat

Chronic windows permitted longitudinal extracellular glutamate imaging with high spatial resolution and temporal kinetics. We therefore used a repeated imaging design with iGluSnFR mice, acquiring spontaneous cortical activity data before initiating the CSD protocol and then once again at its conclusion. This allowed us to examine change in connection strength related to the CSD and its control condition (Fig. 2A and B). Our analyses revealed an increased region of interest functional connection strength as a consequence of the CSD protocol, and a loss of overall connection strength in the control condition. This is illustrated by seed pixel correlation maps showing enlarged territory in defeated, relative to control mice (Fig. 2C and D). This was quantified longitudinally with region of interest correlation values, which revealed a global increase in inter-regional connection strength in defeated animals (Fig. 2E and Supplementary Figs 2 and 3). The estimated cumulative



distribution functions in control animals revealed a loss of connection strength (Fig. 2F and Supplementary Figs 2 and 3).

Optical mapping of regional connectivity after chronic social defeat

To directly probe connectivity, rather than functional correlation, we used viral delivery of ChrimsonR (Supplementary Fig. 4A and B), which allowed 589 nm excitation with minimal cross-talk with 530 nm fluorescence (Supplementary Fig. 4C and D). However, there was weak cross-talk between 470 nm excitation (required for iGluSnFR imaging) and ChrimsonR (Supplementary Fig. 4D and E), most likely due to overexpression and the excitation light required to achieve our temporal sampling. Nevertheless, we were able to optically evoke responses with the expected regionally connected motifs (Lim *et al.*, 2012). Mice underwent mapping at baseline and at the conclusion of the CSD protocol with identical laser parameters. In the Ai85 mouse, longitudinal mapping revealed increased maximal $\Delta F/F_0$ responses in associated regions

of interest after parietal temporal association stimulation in defeated animals compared to controls (Supplementary Fig. 4F; plotted as a difference from baseline), but not after retrosplenial stimulation (Supplementary Fig. 4G). We sought to confirm this with second indicator, the intracellular calcium sensor, GCaMP6s in the Ai94 mouse (Chen *et al.*, 2013; Madisen *et al.*, 2015). Longitudinal mapping in the Ai94 mouse once again revealed similarly increased maximal $\Delta F/F_0$ responses in defeated animals compared to controls after parietal temporal association stimulation (Supplementary Fig. 4H), but not after retrosplenial stimulation (Supplementary Fig. 4I).

Increased regional voltage sensitive dye functional correlation after chronic social defeat

To validate the functional Ai85 CSD phenotype, we imaged an independent cohort of mice having undergone CSD and control conditions (Fig. 3A) using VSD (Mohajerani *et al.*, 2010; Chan *et al.*, 2015). This approach permits mesoscale quantification of electrical activity in the brain in the absence of haemodynamic confounds. The CSD protocol

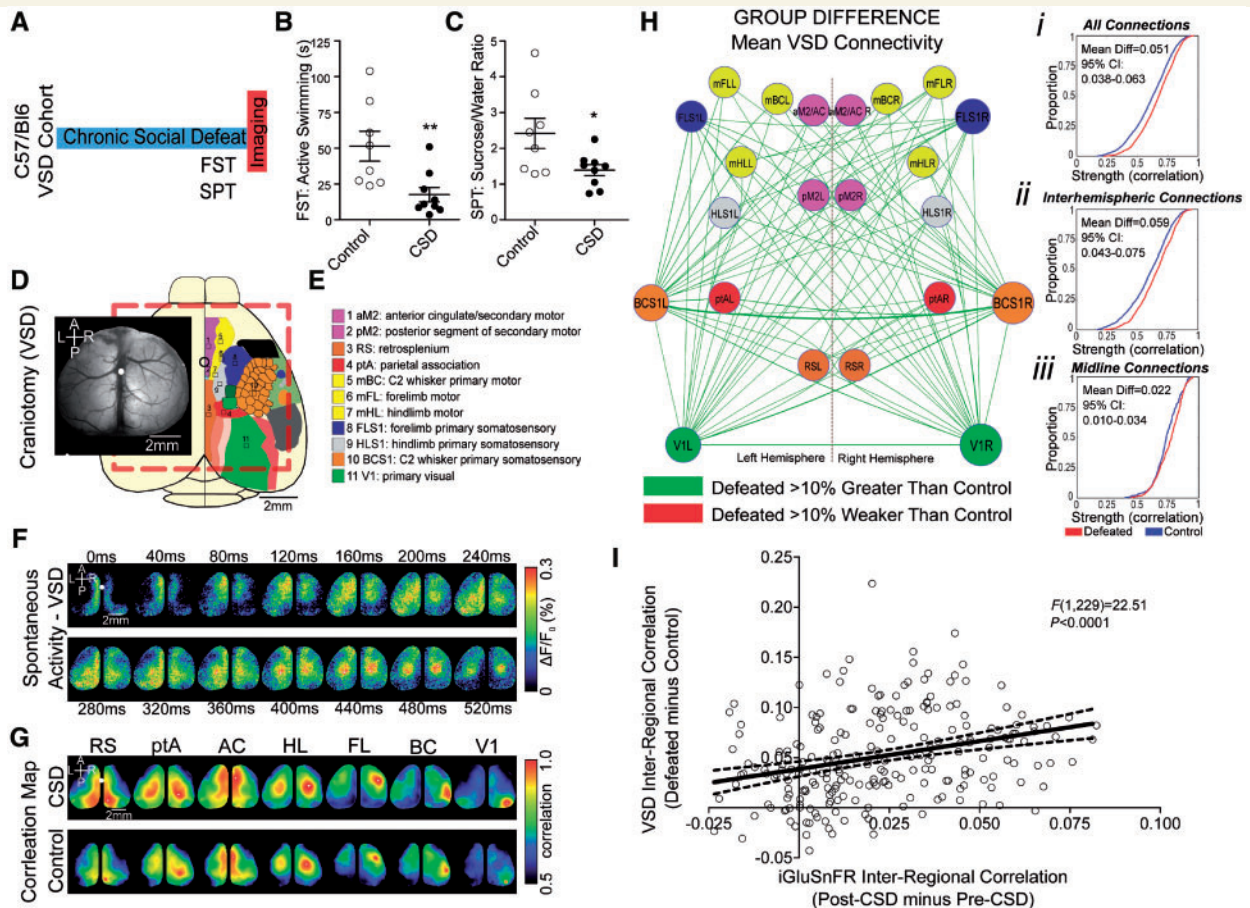


Figure 3 Validation of the functional inter-regional correlation phenotype associated with CSD using VSD. (A) Schematic illustrating the experimental design. (B) CSD results in depression-like behaviour as measured by the FST [Control $n = 8$ versus Defeated $n = 9$, $t(15) = 3.01$, $P = 0.0087$] and (C) the Sucrose Preference Test [SPT; Control $n = 8$ versus Defeated $n = 9$, $t(15) = 2.39$, $P = 0.030$] in C57BL/6J mice. (D) Representative craniotomy exposing the cortex with dura removed in order to incubate VSD. (E) Schematic representation of the regions of interest (ROIs) over a single hemisphere. (F) Montage of spontaneous VSD $\Delta F/F_0$ activity used to derive measures of inter-regional synchrony. (G) Seed pixel correlation maps showing an expansion correlated territories in defeated animals in the VSD cohort. (H) Acute VSD imaging reveals increased functional connection strength in defeated mice compared to control mice ($n = 9$, defeated versus $n = 8$, control): (i) all connections [231 connections/animal; GLMEM group-effect: $t(3925) = 15.72$, $P = 4.38 \times 10^{-54}$]; (ii) interhemispheric connections [121 connections/animal; GLMEM group effect: $t(933) = 7.71$, $P = 4.38 \times 10^{-14}$]; and (iii) midline connections [28 connections/animal; GLMEM group effect: $t(474) = 2.98$, $P = 0.0029$]. (I) Inter-regional correlation strengths related to the CSD protocol using iGluSnFR and VSD were correlated [$F(1,229) = 22.51$, $P < 0.0001$], suggesting a common effect captured using these different sensors and approaches. 95% confidence intervals (95% CI) derived from bootstrapped analyses. *ns* = not significant.

resulted in depressive-like behaviour in this independent cohort as determined with the Forced Swim Test (Fig. 3B) and Sucrose Preference Test (Fig. 3C). A representative craniotomy permitting incubation of VSD over the cortex is illustrated in Fig. 3D, in conjunction with the 22 regions of interest quantified through correlation of spontaneous cortical activity (Fig. 3E). A montage typifying the $\Delta F/F_0$ signal used to quantify region of interest VSD functional correlation is illustrated in Fig. 3F.

The group comparison of VSD preparations after CSD revealed global increase in the correlation of regions of interest activity, as illustrated by the enlarged territory in seed pixel correlation maps (Fig. 3G). This was quantified with region of interest correlation values (Fig. 3H and Supplementary Fig. 5).

Linear regression revealed a significant concordance between group differences in VSD connection strengths and longitudinal change after CSD identified with iGluSnFR (Fig. 3I). As these two sensors produce related, but distinct, signals in addition to chronic as opposed to cross-sectional group differences, perfect agreement is not expected. Therefore, a modest but highly significant correlation between the findings ensuing from these two approaches suggests a common biological phenomenon.

Acute effects of ketamine on extracellular glutamate

We then challenged defeated and control iGluSnFR mice with subanaesthetic ketamine (10 mg/kg or 50 mg/kg,

intraperitoneal). The rapid kinetics of this sensor allows the specific detection of real-time extracellular glutamate signals *in vivo, in situ* (Marvin *et al.*, 2013). We observed a large gain in extracellular glutamate in defeated animals after a 50 mg/kg dose, as indicated by sustained increases in iGluSnFR fluorescence (Fig. 4A), but not after ketamine 10 mg/kg or vehicle (Fig. 4B). A 50 mg/kg dose of ketamine in Thy1-GFP mice (activity-independent fluorescence) (Vanni and Murphy, 2014) resulted in a modest loss of fluorescence (Fig. 4C and Supplementary Fig. 6A), presumably related to oxy- and deoxyhaemoglobin's absorption spectrum that includes a peak at 530 nm (Ma *et al.*, 2016) and ketamine's known haemodynamic effects. Therefore, stable iGluSnFR fluorescence in control mice may indicate increased extracellular glutamate (Moghaddam *et al.*, 1997; Homayoun and Moghaddam, 2007; Chowdhury *et al.*, 2017). An anaesthetic dose of ketamine revealed stable iGluSnFR fluorescence (Fig. 4D and Supplementary Fig. 6B), suggesting specificity to chronic stress rather than sensitivity to ketamine.

Yet, as the phenotype could simply be attributable to an effect of compounded anaesthesia after chronic stress, we challenged a set of animals with midazolam (Fig. 4G and Supplementary Fig. 6C) or a higher concentration of isoflurane (3%; Fig. 4H and Supplementary Fig. 6D) and did not observe the unique rapidly increasing iGluSnFR fluorescence noted with 50 mg/kg of subanaesthetic ketamine.

Further, the temporal resolution of the iGluSnFR signal revealed fluorescence transients, particularly in defeated animals, after subanaesthetic ketamine (Fig. 4E). We quantified these 15 min after administration when iGluSnFR fluorescence had stabilized, and found more transients in defeated animals (Fig. 4F). Midazolam (Fig. 4G) and deep isoflurane anaesthesia (Fig. 4H) experiments did not reveal such transients. These experiments instead suggested a suppression of iGluSnFR signal variability with anaesthetic depth. The global phenomenon in defeated animals was most pronounced in somatosensory cortex (Fig. 4I and J).

As excitatory amino acid transporters are highly efficient at clearing extrasynaptic glutamate (Bridges and Esslinger, 2005), we considered whether the defeated glutamate phenotype unmasked by ketamine may reflect impaired glutamate transporter function after chronic stress (Popoli *et al.*, 2011), as identified in post-mortem samples from hippocampus and cortex of depressed humans (Sequeira *et al.*, 2009; Medina *et al.*, 2013) and murine models of depression (Zink *et al.*, 2010; Zhang *et al.*, 2013). Indeed, glial glutamate transporter deficiencies across key regions, such as the prefrontal cortex (Birey *et al.*, 2015) and habenula (Cui *et al.*, 2014), produce depressive-like behaviour, and therefore ketamine may be interacting with a local cortical alteration. Thus, we performed bilateral craniotomies in naïve iGluSnFR mice and incubated the transporter blocker DL-TBOA (500 μ M) over one hemisphere and control solution over the contralateral hemisphere. The iGluSnFR dose-dependent increase in fluorescence

(Fig. 4K and L) and fluorescence transients (Fig. 4M and N) observed in defeated animals was replicated in DL-TBOA-treated hemispheres.

Acute effects of ketamine on iGluSnFR functional correlation

The inter-regional correlation changes 15 min after the administration of ketamine were compared to their vehicle-treated counterparts, allowing a comparison of the acute effects of ketamine. Consistent with large global iGluSnFR transients observed in the ketamine-treated groups, a large increase in the correlation between regional iGluSnFR signals was noted across groups and at both doses (Fig. 5A–D and Supplementary Fig. 7).

Change in iGluSnFR functional correlation after 24 h

Longitudinal testing with the TST suggested that in the absence of subanaesthetic ketamine, defeated and control animals had increased immobility time (Fig. 6A and B). Ketamine treatment instead decreased immobility time, however, this was only statistically significant for defeated animals (Fig. 6B). Moreover, the number of iGluSnFR transients identified during the acute administration of ketamine significantly predicted magnitude of the antidepressant response (Fig. 6C); however, this was only at a trend level when including animals for whom no transients were identified [$F(1,45) = 3.92$, $P = 0.0538$].

In comparison to their respective vehicle-treated comparators, at 24 h we observed a reduction in functional correlation in defeated animals treated with both 10 mg/kg (Fig. 6D and Supplementary Fig. 8A) and 50 mg/kg (Fig. 6E and Supplementary Fig. 8B) of ketamine. The connection strength changes in defeated animals treated with 10 mg/kg were only weakly anticorrelated with the connection strengths that changed as a result of CSD stress (Fig. 7A), whereas in the connection strengths associated with 50 mg/kg in defeated animals were strongly anti-correlated with CSD-related changes (Fig. 7B). Conversely, there was a divergent effect in control animals, whereby the 10 mg/kg dose of ketamine resulted in an increase in functional correlation (Fig. 6F and Supplementary Fig. 8C) and the 50 mg/kg dose of ketamine resulted in a decrease in functional correlation (Fig. 6G and Supplementary Fig. 8D), similar to that observed in defeated animals.

To ensure specificity to subanaesthetic and thus antidepressant doses, we examined changes 24 h after an anaesthetic dose of ketamine (100 mg/kg) that has not been associated with antidepressant-like effects (Li *et al.*, 2010). We found no significant changes in region of interest correlation strength (Supplementary Fig. 9).

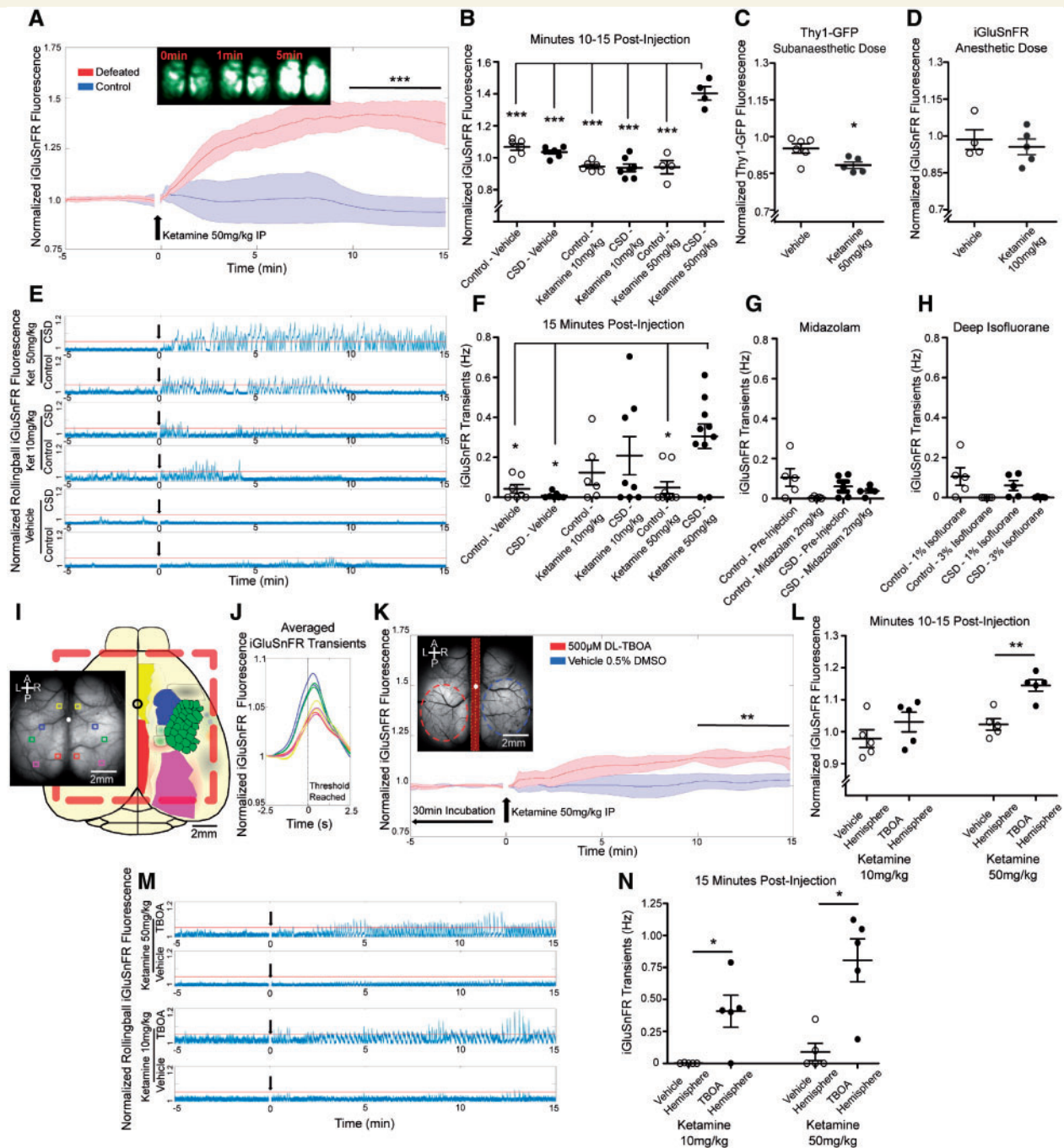


Figure 4 Subanaesthetic ketamine produces a unique extracellular glutamate phenotype in defeated animals. **(A)** Defeated animals have a rapid increase in iGluSnFR (extracellular glutamate sensor) fluorescence after 50 mg/kg of ketamine [10–15 min: Defeated $n = 4$, 1.40 ± 0.04 versus Control $n = 4$, 0.94 ± 0.04 , $t(6) = 7.85$, $P = 0.0002$]. The inset illustrates a montage of iGluSnFR fluorescence from a defeated animal after ketamine injection (immediately after injection, after 1 min and after 5 min). **(B)** iGluSnFR fluorescence significantly increased for defeated animals receiving 50 mg/kg of ketamine, but remained constant for all other groups [$F(5,33) = 44.22$, $P < 0.0001$; Dunnett *post hoc* illustrated]. **(C)** Subanaesthetic ketamine (50 mg/kg) results in decreased fluorescence in Thy1-GFP mice, chosen for its activity-independent blue-green fluorescence [10–15 min: ketamine $n = 5$, 0.88 ± 0.01 versus saline $n = 5$, 0.95 ± 0.01 , $t(8) = 2.83$, $P = 0.0197$]. **(D)** Anaesthetic doses of ketamine (100 mg/kg) do not affect iGluSnFR fluorescence [10–15 min: ketamine $n = 4$, 0.98 ± 0.04 versus saline $n = 5$, 0.95 ± 0.03 ; $t(7) = 0.58$, $P = 0.57$]. **(E)** iGluSnFR fluorescence traces in blue after rolling ball filtering together with the threshold in red illustrating the onset of transients after ketamine or vehicle administration. Though these examples demonstrate the abatement of transients in control animals receiving both 10 mg/kg and 50 mg/kg of subanaesthetic ketamine and defeated animals receiving 10 mg/kg, transients persisted in some animals. **(F)** Defeated mice receiving 50 mg/kg have an increased number of threshold transients after 15 min [$F(5,41) = 4.50$, $P = 0.0023$; Tukey *post hoc* comparisons illustrated]. **(G)** Midazolam administration did not result in transients in defeated [paired t -test: $t(4) = 1.14$, *ns*] or control animals [paired t -test: $t(4) = 2.36$, *ns*]. **(H)** Deep isoflurane anaesthesia did not result in transients in defeated [paired t -test: $t(4) = 2.33$, *ns*] or control animals [paired

(continued)

Discussion

Our *in vivo* mesoscale imaging recapitulates many large scale functional alterations observed in human major depressive disorder using a robust mouse model of depression and a high spatial-temporal resolution extracellular glutamate sensor. We find global functional alterations after CSD and a unique sensitivity to subanaesthetic ketamine in defeated mice reflected in a global cortical accumulation of glutamate with superimposed glutamate transients. Accordingly, we find global normalization of aberrant glutamate regional functional correlation after challenge with the rapid acting antidepressant, ketamine, proportional to the changes that resulted from CSD stress. The network alterations are widely expressed across cortex, however, they were most notable for multimodal association cortices that are key components of the default mode network. Not only do these regions receive reciprocal projections from nodes essential to ketamine's antidepressant-like effects (Vann *et al.*, 2009), they have been directly implicated in motivational behaviour (Vann *et al.*, 2009) and emotional processes (Maddock, 1999).

The default mode network is a large-scale network involving interactions between multiple association regions. In humans, this network's activity is proportional to postero-medial concentrations of glutamate (Kapogiannis *et al.*, 2013) and is involved in processes requiring internal representation, such as autobiographical memory, imagining the future, or navigation and implicates parietal-temporal junction, medial-temporal, posterior cingulate, and retrosplenial cortex (Spreng *et al.*, 2009). The overactivation of the default network in humans is a consistent finding in depression and is hypothesized to underlie the phenomenon of pathological introspection and depressive rumination (Hamilton *et al.*, 2015; Kaiser *et al.*, 2015) as well as impaired switching between egocentric and allosteric frameworks (Vann *et al.*, 2009). Our data from a murine model of chronic stress are consistent with this interpretation, and longitudinal optical mapping demonstrated loss of regional selectivity for the parietal temporal association cortex, a key multimodal association region.

Humans are hypothesized to have had a preferential expansion in association areas enabling a departure from serial hierarchical circuit functions to allow the development of these parallel functions (Buckner and Krienen,

2013). Yet, emerging evidence in rodents supports the presence of resting state networks (White *et al.*, 2011) and a default mode network (Lu *et al.*, 2012) involving analogous regions, notably the retrosplenial and parietal-temporal association cortex visualized in our methodology. The recapitulation of functional hyperconnectivity in a mouse model of depression and loss of association region selectivity raises the intriguing possibility that this large-scale network phenotype represents a conserved response to chronic adversity. This has been recently suggested in a rodent model of chronic restraint (Henckens *et al.*, 2015). Indeed, an evolutionary role for attention, arousal threat detection, and internal monitoring has been proposed for the constitutively active regions of the default network (Gusnard and Raichle, 2001), consistent with our longitudinally demonstrated increase in correlated activity associated with the CSD model.

Though human major depressive disorder is a complex multidetermined pathological process, it is believed to result, in part, from chronic stress, resulting in neurotoxicity, neuronal atrophy, impaired synaptogenesis and NMDA receptor dysfunction (Liu and Aghajanian, 2008). The mechanism of ketamine's rapid antidepressant effects is incompletely understood, yet appears to be neuronal activity dependent (Fuchikami *et al.*, 2015; Carreno *et al.*, 2016), resulting in increased BDNF (Autry *et al.*, 2011) and synaptogenesis (Li *et al.*, 2010; Autry *et al.*, 2011). It appears to exert effects through NMDA receptors, but also through non-NMDA receptor mechanisms (Zanos *et al.*, 2016). Moreover, increasing evidence suggests that several interacting brain regions are essential to ketamine's antidepressant effects, notably the ventral hippocampus (Carreno *et al.*, 2016) and medial prefrontal infralimbic cortex (Fuchikami *et al.*, 2015). Other brain regions important in depression, for instance the lateral habenula, where increased activity related to dysregulated glutamate-GABA balance produces a depression-like phenotype (Shabel *et al.*, 2014), appear to be implicated in the acute effects of ketamine in humans (Carlson *et al.*, 2013). Our data support the hypothesis that subanaesthetic ketamine simultaneously affects connected nodes within a distributed network of depression.

Increased glutamate release after ketamine has been implicated in animals (Moghaddam *et al.*, 1997; Chowdhury *et al.*, 2012, 2017) and humans (Stone *et al.*, 2012; Milak *et al.*, 2016); however, our characterization is

Figure 4 Continued

t-test: $t(4) = 2.36$, *ns*). (I) Schematic illustrating location of (J) averaged traces crossing threshold demonstrating a global cortical function strongest in somatosensory regions. (K) Naïve Ai85 female animals received two craniotomies separated by a dental cement barrier (illustrated in the inset). The DL-TBOA treated hemisphere exhibited higher normalized iGluSnFR fluorescence after 50 mg/kg ketamine. (L) Compared to the contralateral vehicle-treated hemisphere, the hemispheres treated with 500 μ M DL-TBOA recapitulate increased iGluSnFR fluorescence after 50 mg/kg of ketamine [$n = 5$ mice; TBOA 1.14 ± 0.01 versus Vehicle 1.02 ± 0.01 , paired *t*-test: $t(4) = 7.41$, $P = 0.0018$] but not 10 mg/kg [$n = 5$ mice; paired *t*-test: $t(4) = 2.29$, *ns*]. (N) The hemispheres treated with 500 μ M DL-TBOA recapitulate iGluSnFR transients with both 10 mg/kg [$n = 5$ mice; DL-TBOA 0.40 ± 0.12 versus Vehicle 0.00 ± 0.00 , paired *t*-test: $t(4) = 3.27$, $P = 0.030$] and 50 mg/kg [$n = 5$ mice; DL-TBOA 0.80 ± 0.16 versus Vehicle 0.08 ± 0.06 , paired *t*-test: $t(4) = 3.86$, $P = 0.018$] of ketamine. *ns* = not significant.

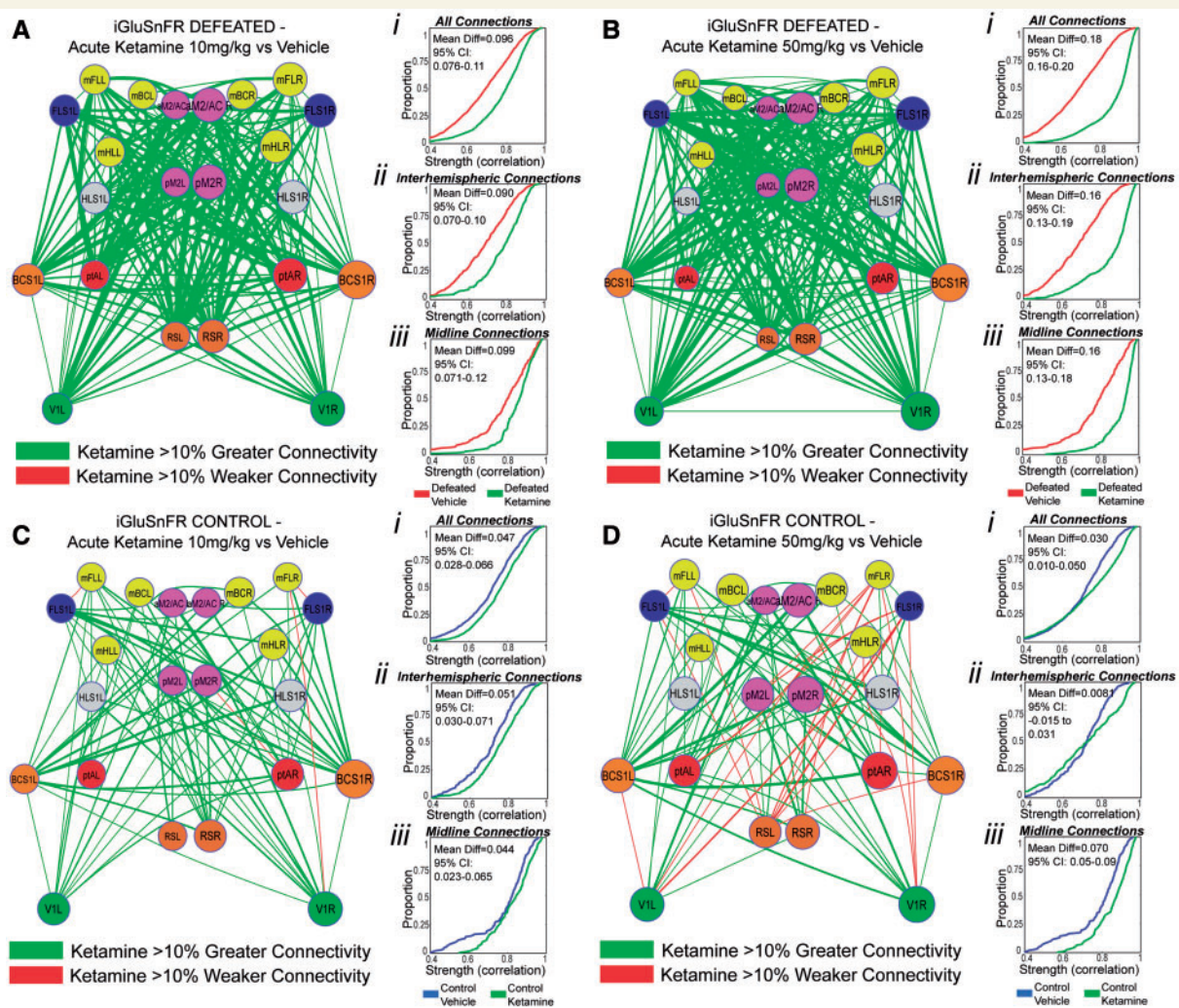


Figure 5 Acute effects (15 min post-administration) of subanaesthetic ketamine on iGluSnFR regional correlations. We present changes in defeated animals after two subanaesthetic doses of ketamine (10 mg/kg and 50 mg/kg) in the *top* panels and changes in control animals to the same doses in the *bottom* panels. Comparisons reflect differences from vehicle-treated animals. **(A)** Network diagram representing increased correlation strength during acute ketamine (10 mg/kg) administration in defeated animals ($n = 7$, vehicle-treated versus $n = 7$, ketamine 10 mg/kg treated): (i) all connections [231 connections/animal; GLMEM CSD-10 mg/kg, $t(3232) = 22.27$, $P = 2.17 \times 10^{-102}$]; (ii) interhemispheric connections [121 connections/animal; GLMEM CSD-10 mg/kg, $t(768) = 9.98$, $P = 3.86 \times 10^{-22}$]; and (iii) midline connections [28 connections/animal; GLMEM CSD-10 mg/kg, $t(390) = 6.09$, $P = 2.58 \times 10^{-9}$]. **(B)** An elevated subanaesthetic dose of ketamine (50 mg/kg) resulted in large increases in regional correlation strength in defeated animals ($n = 7$, vehicle-treated versus $n = 9$, ketamine 50 mg/kg treated): (i) all connections [231 connections/animal; GLMEM CSD-50 mg/kg, $t(3694) = 46.49$, $P < 2.22 \times 10^{-308}$]; (ii) interhemispheric connections [121 connections/animal; GLMEM CSD-50 mg/kg, $t(878) = 19.78$, $P = 2.35 \times 10^{-72}$]; and (iii) midline connections [28 connections/animal; GLMEM CSD-50 mg/kg, $t(446) = 11.11$, $P = 1.62 \times 10^{-25}$]. **(C)** Ketamine 10 mg/kg also resulted in increases in regional correlation strength in control animals ($n = 5$, vehicle-treated versus $n = 6$, ketamine 10 mg/kg treated): (i) all connections (231 connections/animal; GLMEM Control-10 mg/kg, $t(2539) = 12.03$, $P = 1.77 \times 10^{-32}$); (ii) interhemispheric connections [121 connections/animal; GLMEM Control-10 mg/kg, $t(603) = 5.77$, $P = 1.75 \times 10^{-8}$]; and (iii) midline connections [28 connections/animal; GLMEM Control-10 mg/kg, $t(306) = 3.69$, $P = 2.64 \times 10^{-4}$]. **(D)** Similarly, an elevated subanaesthetic dose of ketamine (50 mg/kg) resulted in increases in regional correlation strength in control animals ($n = 5$, vehicle-treated versus $n = 8$, ketamine 50 mg/kg treated): (i) all connections [231 connections/animal; GLMEM Control-50 mg/kg, $t(3001) = 6.70$, $P = 2.45 \times 10^{-11}$]; (ii) interhemispheric connections [121 connections/animal; GLMEM Control-50 mg/kg, $t(713) = 1.29$, *ns*]; and (iii) midline connections [28 connections/animal; GLMEM Control-50 mg/kg, $t(362) = 6.42$, $P = 4.05 \times 10^{-10}$]. 95% CI derived from bootstrapped analyses. *ns* = not significant.

the first to achieve *in situ* simultaneous real-time measurement over a large expanse of cortex. Moreover, the temporal resolution afforded by iGluSnFR revealed global surges of glutamate across cortex, most pronounced and sustained in mice having undergone CSD. NMDA receptor

antagonism has been associated with thalamic-gated cortical and hippocampal delta bursting (Zhang *et al.*, 2009, 2012), and rapid increase in delta power seen with subanaesthetic ketamine (Zhang *et al.*, 2012) is consistent with the onset of iGluSnFR transients and cortical glutamate

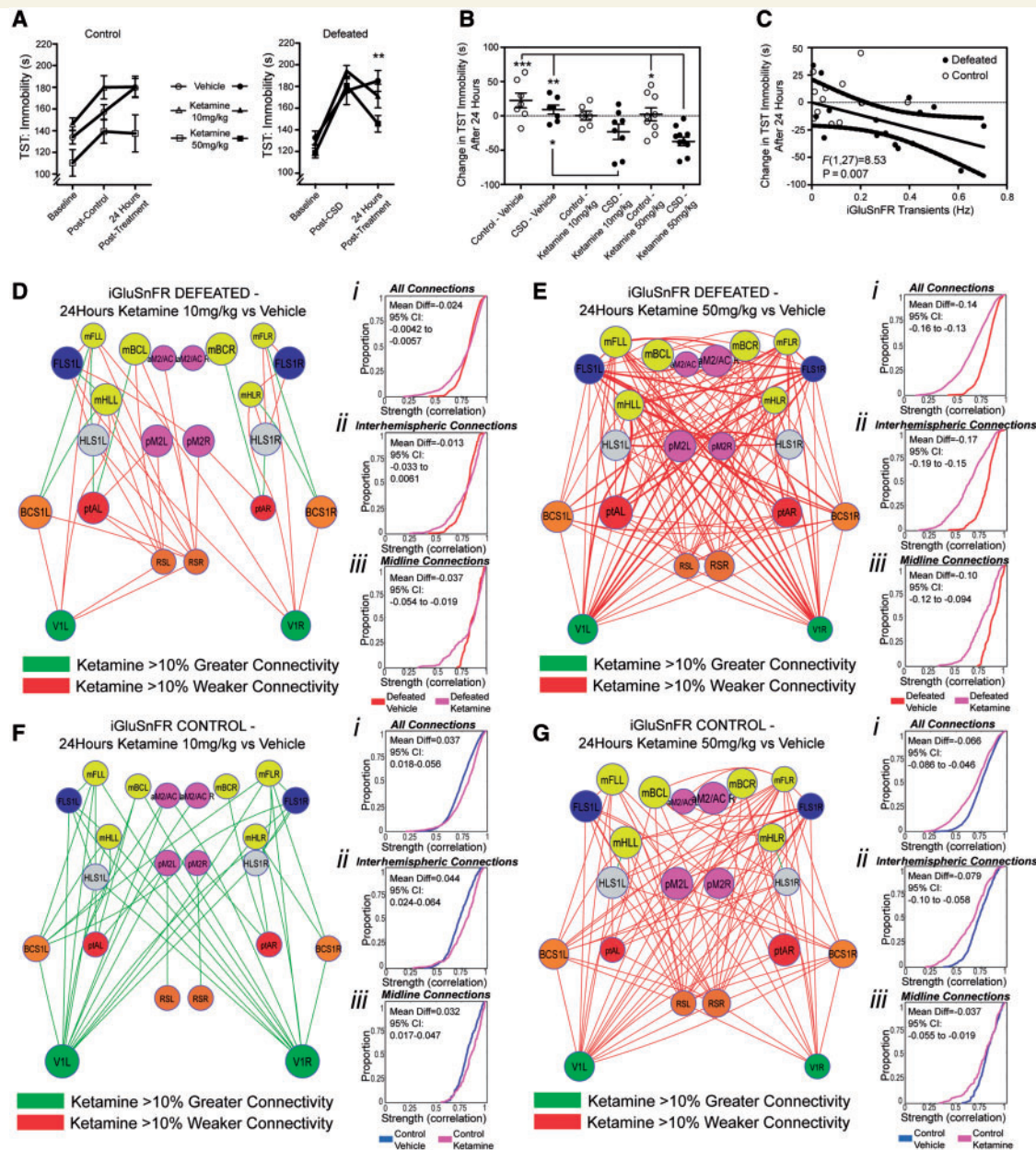


Figure 6 Behavioural and iGluSnFR regional correlation changes 24 h after the administration of subanaesthetic ketamine. (A) There was no significant TST treatment \times Time interaction in control animals [$F(4,38) = 0.95, P = 0.44$], however defeated animals had an antidepressant-like response to ketamine after 24 h [$F(4,44) = 3.15, P = 0.022$; Bonferroni *post hoc*]. (B) Change in TST performance reveals decreases in immobility in defeated animals after ketamine [$F(5,46) = 6.31, P = 0.0002$; Tukey *post hoc*]. (C) Ketamine-induced iGluSnFR transients predicted change on the TST [$F(1,27) = 8.53, P = 0.0007$]. (D) Network diagram representing decreased correlation strength in defeated animals 24 h after ketamine ($n = 5$, vehicle versus $n = 8$, ketamine 10 mg/kg): (i) all connections [231 connections/animal; GLMEM CSD-10 mg/kg, $t(3001) = 5.84, P = 5.76 \times 10^{-9}$]; (ii) interhemispheric connections [121 connections/animal; GLMEM CSD-10 mg/kg, $t(713) = 1.88, ns$]; and (iii) midline connections [28 connections/animal; GLMEM CSD-10 mg/kg, $t(362) = 3.14, P = 0.0018$]. (E) Network diagram representing decreased correlation strength in defeated animals 24 h after ketamine ($n = 5$, vehicle versus $n = 7$, ketamine 50 mg/kg): (i) all connections [231 connections/animal; GLMEM CSD-50 mg/kg, $t(2770) = 36.05, P = 9.50 \times 10^{-234}$]; (ii) interhemispheric connections [121 connections/animal; GLMEM CSD-50 mg/kg, $t(658) = 17.87, P = 1.16 \times 10^{-58}$]; and (iii) midline connections [28 connections/animal; GLMEM CSD-50 mg/kg, $t(334) = 11.41, P = 1.07 \times 10^{-25}$]. (F) Network diagram representing increased correlation strength in control animals after 24 h ($n = 7$, vehicle versus $n = 6$, ketamine 10 mg/kg): (i) all connections [231 connections/animal; GLMEM Control-10 mg/kg, $t(3001) = 10.14, P = 8.18 \times 10^{-24}$]; (ii) interhemispheric connections [121 connections/animal; GLMEM Control-10 mg/kg, $t(713) = 5.90, P = 5.34 \times 10^{-9}$]; and (iii) midline connections [28 connections/animal; GLMEM Control-10 mg/kg, $t(362) = 3.77, P = 1.89 \times 10^{-4}$]. (G) Network diagram representing decreased correlation strength in control animals ($n = 7$, vehicle treated versus $n = 8$, ketamine 50 mg/kg): (i) all connections [231 connections/animal; GLMEM Control-50 mg/kg, $t(3463) = 17.03, P = 1.41 \times 10^{-62}$]; (ii) interhemispheric connections [121 connections/animal; GLMEM Control-50 mg/kg, $t(823) = 8.84, P = 5.29 \times 10^{-18}$]; and (iii) midline connections [28 connections/animal; GLMEM Control-50 mg/kg, $t(413) = 3.74, P = 2.06 \times 10^{-4}$]. 95% CI derived from bootstrapped analyses. *ns* = not significant.

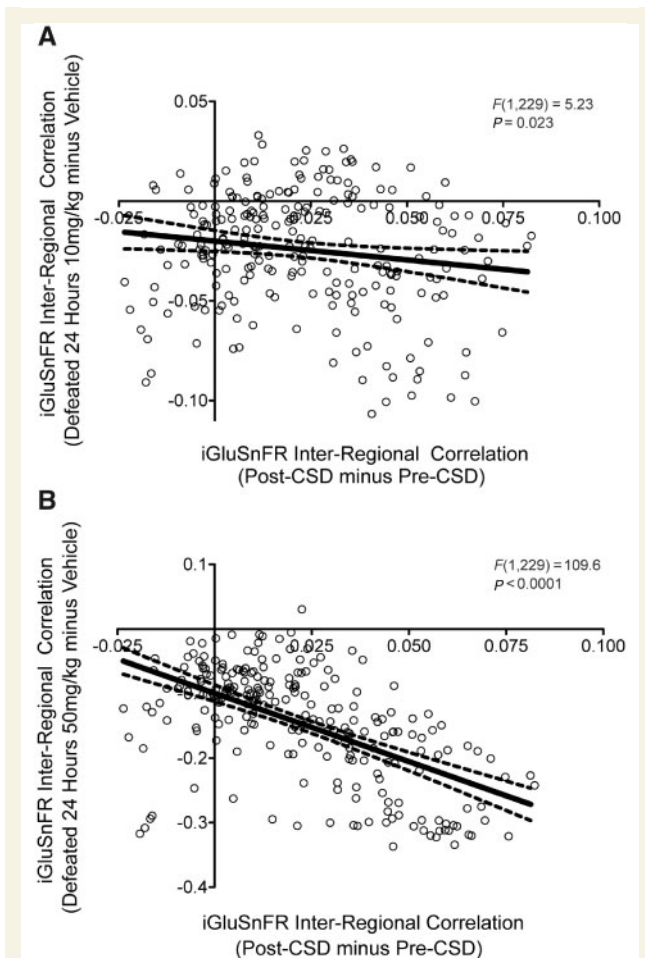


Figure 7 Subanaesthetic ketamine rectifies aberrant inter-regional connectivity resulting from CSD in proportion to its antidepressant-like effects. In both panels, the longitudinal change in inter-regional correlations related to the CSD protocol are plotted against the changes observed after 24 h in the ketamine treated groups compared to saline treated group. **(A)** Inter-regional correlation changes associated with the 10 mg/kg group were weakly, yet statistically significantly, anticorrelated with CSD-related changes [$F(1,229) = 5.23, P = 0.023$]. **(B)** The 50 mg/kg treated group, which demonstrated a more robust antidepressant-like effect, revealed changes in inter-regional correlation that were strongly anticorrelated with CSD-related changes [$F(1,229) = 109.6, P < 0.0001$].

accumulation. Our findings suggest that local cortical alterations in glutamate signalling and reuptake resulting from chronic stress (Popoli *et al.*, 2011) likely play an important role downstream of subanaesthetic ketamine's actions on the thalamus (Zhang *et al.*, 2009, 2012), the ventral hippocampus (Carreno *et al.*, 2016) and the infralimbic prefrontal cortex (Fuchikami *et al.*, 2015). Indeed, the global accumulation of glutamate observed in defeated mice may underlie cortex-wide increases in trophic factors (Autry *et al.*, 2011) rectifying a global cortical synaptogenic deficit after chronic stress (Duman and Aghajanian, 2012).

Succinctly, our data suggest increased cortical regionally correlated activity and unique sensitivity to subanaesthetic ketamine after CSD stress. We observed pathological and treatment effects that were not localized within a single cortical network but expressed globally, with a major role for multimodal association cortices of the default mode network.

Acknowledgements

We would like to thank Pumin Wang for surgical assistance and Cindy Jiang for colony management and genotyping. Vancouver Coastal Health and the University of British Columbia Psychiatry Research Track residency program provided AM with protected research time.

Funding

Canadian Institutes of Health Research (CIHR) foundation grant FDN-143209 to T.H.M. and Canadian Neurophotonics platform Support from Brain Canada to T.H.M. A.M. is a CIHR Vanier Scholar.

Supplementary material

Supplementary material is available at *Brain* online.

References

- Autry AE, Adachi M, Nosyreva E, Na ES, Los MF, Cheng PF, et al. NMDA receptor blockade at rest triggers rapid behavioural antidepressant responses. *Nature* 2011; 475: 91–5.
- Birey F, Kloc M, Chavali M, Hussein I, Wilson M, Christoffel DJ, et al. Genetic and stress-induced loss of NG2 Glia triggers emergence of depressive-like behaviors through reduced secretion of FGF2. *Neuron* 2015; 88: 941–56.
- Bridges RJ, Esslinger CS. The excitatory amino acid transporters: pharmacological insights on substrate and inhibitor specificity of the EAAT subtypes. *Pharmacol Ther* 2005; 107: 271–85.
- Buckner RL, Andrews-Hanna JR, Schacter DL. The brain's default network: anatomy, function, and relevance to disease. *Ann N Y Acad Sci* 2008; 1124: 1–38.
- Buckner RL, Krienen FM. The evolution of distributed association networks in the human brain. *Trends Cogn Sci* 2013; 17: 648–65.
- Bullmore E, Sporns O. The economy of brain network organization. *Nat Rev Neurosci* 2012; 13: 336–49.
- Carlson PJ, Diazgranados N, Nugent AC, Ibrahim L, Luckenbaugh DA, Brutsche N, et al. Neural correlates of rapid antidepressant response to ketamine in treatment-resistant unipolar depression: a preliminary positron emission tomography study. *Biol Psychiatry* 2013; 73: 1213–21.
- Carreno FR, Donegan JJ, Boley AM, Shah A, DeGuzman M, Frazer A, et al. Activation of a ventral hippocampus-medial prefrontal cortex pathway is both necessary and sufficient for an antidepressant response to ketamine. *Mol Psychiatry* 2016; 21: 1298–308.
- Chan AW, Mohajerani MH, LeDue JM, Wang YT, Murphy TH. Mesoscale infraslow spontaneous membrane potential fluctuations recapitulate high-frequency activity cortical motifs. *Nat Commun* 2015; 6: 7738.

- Chen TW, Wardill TJ, Sun Y, Pulver SR, Renninger SL, Baohan A, et al. Ultrasensitive fluorescent proteins for imaging neuronal activity. *Nature* 2013; 499: 295–300.
- Chowdhury GM, Behar KL, Cho W, Thomas MA, Rothman DL, Sanacora G. (1)H-[(1)3C]-nuclear magnetic resonance spectroscopy measures of ketamine's effect on amino acid neurotransmitter metabolism. *Biol Psychiatry* 2012; 71: 1022–5.
- Chowdhury GM, Zhang J, Thomas M, Banasr M, Ma X, Pittman B, et al. Transiently increased glutamate cycling in rat PFC is associated with rapid onset of antidepressant-like effects. *Mol Psychiatry* 2017; 22: 120–6.
- Cui W, Mizukami H, Yanagisawa M, Aida T, Nomura M, Isomura Y, et al. Glial dysfunction in the mouse habenula causes depressive-like behaviors and sleep disturbance. *J Neurosci* 2014; 34: 16273–85.
- Duman RS, Aghajanian GK. Synaptic dysfunction in depression: potential therapeutic targets. *Science* 2012; 338: 68–72.
- Fox MD, Raichle ME. Spontaneous fluctuations in brain activity observed with functional magnetic resonance imaging. *Nat Rev Neurosci* 2007; 8: 700–11.
- Fox MD, Zhang D, Snyder AZ, Raichle ME. The global signal and observed anticorrelated resting state brain networks. *J Neurophysiol* 2009; 101: 3270–83.
- Fuchikami M, Thomas A, Liu R, Wohleb ES, Land BB, DiLeone RJ, et al. Optogenetic stimulation of infralimbic PFC reproduces ketamine's rapid and sustained antidepressant actions. *Proc Natl Acad Sci USA* 2015; 112: 8106–11.
- Golden SA, Covington HE, 3rd, Berton O, Russo SJ. A standardized protocol for repeated social defeat stress in mice. *Nat Protoc* 2011; 6: 1183–91.
- Gong Q, He Y. Depression, neuroimaging and connectomics: a selective overview. *Biol Psychiatry* 2015; 77: 223–35.
- Gusnard DA, Raichle ME. Searching for a baseline: functional imaging and the resting human brain. *Nat Rev Neurosci* 2001; 2: 685–94.
- Hamilton JP, Farmer M, Fogelman P, Gotlib IH. Depressive rumination, the default-mode network, and the dark matter of clinical neuroscience. *Biol Psychiatry* 2015; 78: 224–30.
- Henckens MJ, van der Marel K, van der Toorn A, Pillai AG, Fernandez G, Dijkhuizen RM, et al. Stress-induced alterations in large-scale functional networks of the rodent brain. *Neuroimage* 2015; 105: 312–22.
- Homayoun H, Moghaddam B. NMDA receptor hypofunction produces opposite effects on prefrontal cortex interneurons and pyramidal neurons. *J Neurosci* 2007; 27: 11496–500.
- Horowitz SG, Fukunaga M, de Zwart JA, van Gelderen P, Fulton SC, Balkin TJ, et al. Low frequency BOLD fluctuations during resting wakefulness and light sleep: a simultaneous EEG-fMRI study. *Hum Brain Mapp* 2008; 29: 671–82.
- Kaiser RH, Andrews-Hanna JR, Wager TD, Pizzagalli DA. Large-scale network dysfunction in major depressive disorder: a meta-analysis of resting-state functional connectivity. *JAMA Psychiatry* 2015; 72: 603–11.
- Kapogiannis D, Reiter DA, Willette AA, Mattson MP. Posteromedial cortex glutamate and GABA predict intrinsic functional connectivity of the default mode network. *Neuroimage* 2013; 64: 112–9.
- Klapoetke NC, Murata Y, Kim SS, Pulver SR, Birdsey-Benson A, Cho YK, et al. Independent optical excitation of distinct neural populations. *Nat Methods* 2014; 11: 338–46.
- Li N, Lee B, Liu RJ, Banasr M, Dwyer JM, Iwata M, et al. mTOR-dependent synapse formation underlies the rapid antidepressant effects of NMDA antagonists. *Science* 2010; 329: 959–64.
- Lim DH, LeDue JM, Mohajerani MH, Murphy TH. Optogenetic mapping after stroke reveals network-wide scaling of functional connections and heterogeneous recovery of the peri-infarct. *J Neurosci* 2014; 34: 16455–66.
- Lim DH, LeDue JM, Murphy TH. Network analysis of mesoscale optical recordings to assess regional, functional connectivity. *Neurophotonics* 2015; 2: 041405.
- Lim DH, Mohajerani MH, Ledue J, Boyd J, Chen S, Murphy TH. *In vivo* large-scale cortical mapping using channelrhodopsin-2 stimulation in transgenic mice reveals asymmetric and reciprocal relationships between cortical areas. *Front Neural Circuits* 2012; 6: 11.
- Liu R-J, Aghajanian GK. Stress blunts serotonin- and hypocretin-evoked EPSCs in prefrontal cortex: role of corticosterone-mediated apical dendritic atrophy. *Proc Natl Acad Sci USA* 2008; 105: 359–64.
- Lu H, Zou Q, Gu H, Raichle ME, Stein EA, Yang Y. Rat brains also have a default mode network. *Proc Natl Acad Sci USA* 2012; 109: 3979–84.
- Luyckx JJ, Laban KG, van den Heuvel MP, Boks MP, Mandl RC, Kahn RS, et al. Region and state specific glutamate downregulation in major depressive disorder: a meta-analysis of (1)H-MRS findings. *Neurosci Biobehav Rev* 2012; 36: 198–205.
- Ma Y, Shaik MA, Kim SH, Kozberg MG, Thibodeaux DN, Zhao HT, et al. Wide-field optical mapping of neural activity and brain haemodynamics: considerations and novel approaches. *Philos Trans R Soc Lond B Biol Sci* 2016; 371.
- Maddock RJ. The retrosplenial cortex and emotion: new insights from functional neuroimaging of the human brain. *Trends Neurosci* 1999; 22: 310–6.
- Madisen L, Garner AR, Shimaoka D, Chuong AS, Klapoetke NC, Li L, et al. Transgenic mice for intersectional targeting of neural sensors and effectors with high specificity and performance. *Neuron* 2015; 85: 942–58.
- Marvin JS, Borghuis BG, Tian L, Cichon L, Harnett MT, Akerboom J, et al. An optimized fluorescent probe for visualizing glutamate neurotransmission. *Nat Methods* 2013; 10: 162–70.
- McGirr A, Berlim MT, Bond DJ, Fleck MP, Yatham LN, Lam RW. A systematic review and meta-analysis of randomized double-blind controlled trials of ketamine in the rapid treatment of major depressive episodes. *Psychol Med* 2015; 45: 693–704.
- Medina A, Burke S, Thompson RC, Bunney W Jr, Myers RM, Schatzberg A, et al. Glutamate transporters: a key piece in the glutamate puzzle of major depressive disorder. *J Psychiatr Res* 2013; 47: 1150–6.
- Menon V. Large-scale brain networks and psychopathology: a unifying triple network model. *Trends Cogn Sci* 2011; 15: 483–506.
- Milak MS, Proper CJ, Mulhern ST, Parter AL, Kegeles LS, Ogden RT, et al. A pilot *in vivo* proton magnetic resonance spectroscopy study of amino acid neurotransmitter response to ketamine treatment of major depressive disorder. *Mol Psychiatry* 2016; 21: 320–7.
- Moghaddam B, Adams B, Verma A, Daly D. Activation of glutamatergic neurotransmission by ketamine: a novel step in the pathway from NMDA receptor blockade to dopaminergic and cognitive disruptions associated with the prefrontal cortex. *J Neurosci* 1997; 17: 2921–7.
- Mohajerani MH, Aminoltejeri K, Murphy TH. Targeted mini-strokes produce changes in interhemispheric sensory signal processing that are indicative of disinhibition within minutes. *Proc Natl Acad Sci USA* 2011; 108: E183–91.
- Mohajerani MH, Chan AW, Mohsenvand M, LeDue J, Liu R, McVea DA, et al. Spontaneous cortical activity alternates between motifs defined by regional axonal projections. *Nat Neurosci* 2013; 16: 1426–35.
- Mohajerani MH, McVea DA, Fingas M, Murphy TH. Mirrored bilateral slow-wave cortical activity within local circuits revealed by fast bihemispheric voltage-sensitive dye imaging in anesthetized and awake mice. *J Neurosci* 2010; 30: 3745–51.
- Popoli M, Yan Z, McEwen BS, Sanacora G. The stressed synapse: the impact of stress and glucocorticoids on glutamate transmission. *Nat Rev Neurosci* 2011; 13: 22–37.
- Porsolt RD, Bertin A, Jalfre M. Behavioral despair in mice: a primary screening test for antidepressants. *Arch Int Pharmacodyn Ther* 1977; 229: 327–36.

- Rubinov M, Sporns O. Complex network measures of brain connectivity: uses and interpretations. *Neuroimage* 2010; 52: 1059–69.
- Rush AJ, Trivedi MH, Wisniewski SR, Nierenberg AA, Stewart JW, Warden D, et al. Acute and longer-term outcomes in depressed outpatients requiring one or several treatment steps: a STAR*D report. *Am J Psychiatry* 2006; 163: 1905–17.
- Sequeira A, Mamdani F, Ernst C, Vawter MP, Bunney WE, Lebel V, et al. Global brain gene expression analysis links glutamatergic and GABAergic alterations to suicide and major depression. *PLoS One* 2009; 4: e6585.
- Shabel SJ, Proulx CD, Piriz J, Malinow R. Mood regulation. GABA/glutamate co-release controls habenula output and is modified by antidepressant treatment. *Science* 2014; 345: 1494–8.
- Silasi G, Xiao D, Vanni MP, Chen AC, Murphy TH. Intact skull chronic windows for mesoscopic wide-field imaging in awake mice. *J Neurosci Methods* 2016; 267: 141–9.
- Smart OL, Tiruvadi VR, Mayberg HS. Multimodal approaches to define network oscillations in depression. *Biol Psychiatry* 2015; 77: 1061–70.
- Spreng RN, Mar RA, Kim AS. The common neural basis of autobiographical memory, prospection, navigation, theory of mind, and the default mode: a quantitative meta-analysis. *J Cogn Neurosci* 2009; 21: 489–510.
- Steru L, Chermat R, Thierry B, Simon P. The tail suspension test: a new method for screening antidepressants in mice. *Psychopharmacology* 1985; 85: 367–70.
- Stone JM, Dietrich C, Edden R, Mehta MA, De Simoni S, Reed LJ, et al. Ketamine effects on brain GABA and glutamate levels with 1H-MRS: relationship to ketamine-induced psychopathology. *Mol Psychiatry* 2012; 17: 664–5.
- Tseng Q, Duchemin-Pelletier E, Deshiere A, Balland M, Guillou H, Filhol O, et al. Spatial organization of the extracellular matrix regulates cell-cell junction positioning. *Proc Natl Acad Sci USA* 2012; 109: 1506–11.
- Vann SD, Aggleton JP, Maguire EA. What does the retrosplenial cortex do? *Nat Rev Neurosci* 2009; 10: 792–802.
- Vanni MP, Murphy TH. Mesoscale transcranial spontaneous activity mapping in GCaMP3 transgenic mice reveals extensive reciprocal connections between areas of somatomotor cortex. *J Neurosci* 2014; 34: 15931–46.
- Vincent JL, Patel GH, Fox MD, Snyder AZ, Baker JT, Van Essen DC, et al. Intrinsic functional architecture in the anaesthetized monkey brain. *Nature* 2007; 447: 83–6.
- White BR, Bauer AQ, Snyder AZ, Schlaggar BL, Lee JM, Culver JP. Imaging of functional connectivity in the mouse brain. *PLoS One* 2011; 6: e16322.
- WHO. The global burden of disease: 2004 update. In: Informatics DoHSA, editor. Geneva: WHO Press; 2008.
- Xie Y, Chan AW, Xue S, Xiao D, Zheng H, Murphy TH. Resolution of high-frequency mesoscale intracortical maps using the genetically-encoded glutamate sensor - iGluSnFR. *J Neurosci* 2016; 36: 1261–72.
- Xu Y, Hackett M, Carter G, Loo C, Galvez V, Glozier N, et al. Effects of low-dose and very low-dose ketamine among patients with major depression: a systematic review and meta-analysis. *Int J Neuropsychopharmacol* 2016; 19.
- Yuksel C, Ongur D. Magnetic resonance spectroscopy studies of glutamate-related abnormalities in mood disorders. *Biol Psychiatry* 2010; 68: 785–94.
- Zanos P, Moaddel R, Morris PJ, Georgiou P, Fischell J, Elmer GI, et al. NMDAR inhibition-independent antidepressant actions of ketamine metabolites. *Nature* 2016; 533: 481–6.
- Zhang XH, Jia N, Zhao XY, Tang GK, Guan LX, Wang D, et al. Involvement of pGluR1, EAAT2 and EAAT3 in offspring depression induced by prenatal stress. *Neuroscience* 2013; 250: 333–41.
- Zhang Y, Llinas RR, Lisman JE. Inhibition of NMDARs in the nucleus reticularis of the thalamus produces delta frequency bursting. *Front Neural Circuits* 2009; 3: 20.
- Zhang Y, Yoshida T, Katz DB, Lisman JE. NMDAR antagonist action in thalamus imposes delta oscillations on the hippocampus. *J Neurophysiol* 2012; 107: 3181–9.
- Zink M, Vollmayr B, Gebicke-Haerter PJ, Henn FA. Reduced expression of glutamate transporters vGluT1, EAAT2 and EAAT4 in learned helpless rats, an animal model of depression. *Neuropharmacology* 2010; 58: 465–73.